THE ASTROPHYSICAL JOURNAL, 465:278–287, 1996 July 1

FOSSIL SIGNATURES OF ANCIENT ACCRETION EVENTS IN THE HALO

KATHRYN V. JOHNSTON, LARS HERNQUIST,[1] AND MICHAEL BOLTE
Board of Studies in Astronomy and Astrophysics, University of California–Santa Cruz, Santa Cruz, CA 95064
Received 1995 November 7; accepted 1996 February 2

ABSTRACT

The role that minor mergers have played in the formation and structure of the Milky Way is still an open question, about which there is much debate. We use numerical simulations to explore the evolution of debris from a tidally disrupted satellite, with the aim of developing a method that can be used to identify and quantify signatures of accretion in a survey of halo stars. For a Milky Way with a spherical halo, we find that debris from minor mergers can remain aligned along great circles throughout the lifetime of the Galaxy. We exploit this result to develop the method of great circle cell counts (GC3), which we test by applying it to artificially constructed halo distributions. Our results suggest that if as few as 1% of the stars in a halo survey are accreted from the disruption of a single subsystem smaller than the Large Magellanic Cloud, GC3 can recover the great circle associated with this debris. The dispersion in GC3 can also be used to detect the presence of structure characteristic of accretion in distributions containing a much smaller percentage of material accreted from any single satellite.

Subject headings: galaxies: interactions — Galaxy: halo — methods: numerical

1. INTRODUCTION

Theories describing the formation of the Milky Way can generally be viewed as variations on or combinations of two scenarios. Based on the kinematics of metal-poor halo field stars, Eggen, Lynden-Bell, & Sandage (1962, hereafter ELS) proposed a model in which the Galaxy began with the free-fall collapse of an approximately uniform, spherical primordial fluctuation. The globular clusters and halo field stars were formed during the free-fall phase, with the bulk of the original Galactic material dissipating energy in the gas phase and falling into a rotationally supported disk. Alternatively, to account for the lack of a metallicity gradient in the halo and the suggestion of a large spread in the ages of outer halo globular clusters, Searle & Zinn (1978, hereafter SZ) proposed a scenario in which the Galaxy was assembled through the gradual merging of many sub-Galactic–sized clouds.

Low-mass stars have life spans that are greater than the age of the Galaxy and do not dissipate orbital energy. Hence, we have an abundance of "fossil" information with which to explore various formation scenarios, through halo stars and clusters, especially their abundances and kinematics. Commonly employed tracers include the kinematics of field stars as a function of [Fe/H] (as in ELS), the age distribution of Galactic globular clusters (see, e.g., Vandenberg, Bolte, & Stetson 1990), trends in cluster age with [Fe/H] and Galactocentric radius (as in SZ), the lack of an abundance gradient with radius or height above the disk, and the persistence of a cold, thin disk (see, e.g., Tóth & Ostriker 1992). (See Larson 1990 and Majewski 1993 for comprehensive reviews.)

Here, we consider the feasibility of probing "fossil" signatures of the formation of the Galaxy through structure in the phase-space distribution of halo field stars. Our approach is motivated by numerical simulations, which demonstrate that distinctive features such as tidal tails are a generic consequence of interactions between comparable mass galaxies (see, e.g., Toomre & Toomre 1972; Barnes 1988, 1992; Hernquist 1992, 1993; Hibbard & Mihos 1995). Similarly, streamers can be produced along the orbit of a satellite galaxy when stars are torn from it by tidal forces from its host (see, e.g., McGlynn 1990; Piatek & Pryor 1995; Johnston, Spergel, & Hernquist 1995) . If such tidal debris were to maintain spatial and kinematic coherence for the lifetime of the Galaxy, then a halo formed through the disruption of many SZ fragments would exhibit streakiness in its phase-space distribution, unlike one originating from a smooth, monolithic collapse, which ought to be mostly featureless.

The possibility that accretion events may leave observable signatures is supported by observations of satellites of the Milky Way that display tantalizing evidence for ongoing tidal interactions. As part of their analysis leading to the discovery of the Sagittarius dwarf galaxy (hereafter Sgr), Ibata, Gilmore, & Irwin (1994) produced an isopleth map of the overdensity of horizontal-branch stars in the region in which the dwarf was thought to lie, which shows highly elongated contours with axis ratios $\sim 3:1$. Grillmair et al. (1995) have also reported the detection of distortions in the outer regions of globular clusters. Both sets of observations are consistent with morphological disturbances produced by tidal perturbations.

Unfortunately, the low surface density of streamers from tidally disturbed objects makes their detection challenging. Nevertheless, it is plausible that stars or satellites that appear to be associated spatially and/or kinematically are indeed debris from tidal interactions. From their simulations of Sgr, Johnston et al. (1995) predict that the tidal streamers associated with this object may be detectable as moving groups in the halo and that if a similar galaxy had been destroyed by the Milky Way within the last gigayear, its remains should still be detectable as a moving group today.

Observational evidence also suggests that there is considerable structure in the phase-space distribution of dwarf galaxy companions in the halo. Lynden-Bell (1976, 1982) was the among the first to note that most of the Milky Way's satellite galaxies lie near two great circles passing close to the Galactic poles. Three dwarf spheroidal galaxies (Draco, Ursa Minor, and Carina) are in the vicinity of the great circle defined by the Small and Large Magellanic

[1] Sloan Foundation Fellow; Presidential Faculty Fellow.

Clouds and the Magellanic Stream (the "Magellanic Plane"), while another five (Fornax, Leo I, Leo II, Sculptor, and Sextans) are distinctly aligned along the "Fornax-Leo-Sculptor Stream." More recently, Lynden-Bell & Lynden-Bell (1995) developed a method to search systematically for coincidences of clusters along great circles and recovered these and several other possible associations of halo objects. Moreover, Lin & Richer (1992), Majewski (1994), and Fusi-Pecci et al. (1995) have shown that several young halo globular clusters are not far from each of these planes, which further supports an interesting physical explanation for these alignments.

Substructure has also been found in the stellar distribution in the halo. Doinidis & Beers (1989) calculated the angular correlation function for the 4400 candidate field horizontal branch stars in a sample covering 2300 deg^2 and found a distinct excess of pairs with angular separations less than 10′. Similar clumpiness has been seen in the phase-space distribution of halo stars in the form of moving groups found in kinematic surveys (see, e.g., Sommer-Larsen & Christiansen 1987; Croswell et al. 1991; Arnold & Gilmore 1992; Majewski, Munn, & Hawley 1994).

However, it is not yet clear to what extent (if at all) the current observations of nonuniform distributions of halo matter reflect the epoch of halo formation, and little attention has been given to procedures suitable for evaluating the phase-space structure of the halo as a whole. In this paper, we begin to examine the nature of debris from tidal interactions employing numerical simulations of the disruption of satellites by the Milky Way. We use our simulations to determine how long substructure from accretion events can persist in the halo. If this timescale is significant (i.e., longer than a few Gyr), we examine the observable properties of the debris. We test various methods for characterizing the substructure on artificial halo distributions, generated from the simulations.

We describe our computational method and explore the behavior of tidal debris in our simulations in § 2. We introduce the method of great circle cell counts and apply it to artificial halo distributions in § 3. Other methods for measuring structure in the halo are discussed in § 4. Finally, we summarize possible implications and limitations of our results in § 5.

2. THE BEHAVIOR OF DEBRIS FROM TIDAL INTERACTIONS

2.1. *Method*

In our simulations, we represent the Milky Way by a rigid potential and model each satellite with a collection of 10^4 self-gravitating particles the mutual interactions of which are calculated using a self-consistent field code (Hernquist & Ostriker 1992). Since the satellite mass is much smaller than that of the Milky Way, dynamical friction and energy exchange are assumed negligible. Interactions between the satellites will occur infrequently, so the evolution of each satellite is considered independently.

A three-component model is used for the Galaxy (Spergel 1996), in which the disk is described by a Miyamoto-Nagai potential (1975), the spheroid by a Hernquist (1990) potential, and the halo by a logarithmic potential:

$$\Phi_{\rm disk} = -\frac{GM_{\rm disk}}{\sqrt{R^2 + (a + \sqrt{z^2 + b^2})^2}}, \quad (1)$$

$$\Phi_{\rm spher} = -\frac{GM_{\rm spher}}{r + c}, \quad (2)$$

$$\Phi_{\rm halo} = v_{\rm halo}^2 \ln (r^2 + d^2). \quad (3)$$

We take $M_{\rm disk} = 1.0 \times 10^{11}$, $M_{\rm spher} = 3.4 \times 10^{10}$, $v_{\rm halo} = 128$, $a = 6.5$, $b = 0.26$, $c = 0.7$, and $d = 12.0$, where masses are in $M_\odot$, velocities are in km s^{-1}, and lengths are in kpc. This choice of parameters yields a nearly flat rotation curve between 1 and 30 kpc and a disk scale height of 0.2 kpc. The radial dependence of the vertical epicyclic frequency of the disk (κ_z) between 3 and 20 kpc is similar to that of an exponential disk with a 4 kpc scale length.

Initially, each satellite is represented by a Plummer (1911) model

$$\Phi = -\frac{GM}{\sqrt{r^2 + r_0^2}}, \quad (4)$$

where M is the mass of the satellite and r_0 is its scale length. The central density of the model is $\rho_0 = 3M/4\pi r_0^3$. Plummer models were chosen because they have flat central density profiles, as do the Milky Way's satellites.

We ran 12 different simulations the properties of which are summarized in Table 1. Columns (2)–(4) of Table 1 give the mass, scale length and central density of the Plummer models. Column (5) gives a characteristic velocity dispersion, σ_c, for each satellite that is calculated from $\sigma_c = (GM/r_0)^{1/2}$. This quantity is interesting because we expect σ_c to affect the rate at which tidal debris from each satellite disperses (see § 2.4). The final column in Table 1 compares the satellite's central density to the average density of the Milky Way within the pericenter of its orbit ($\rho_{\rm Gal}$). Analytic investigations of tidal encounters indicate that the dis-

TABLE 1

MODEL PARAMETERS

Model[a] (1)	M[b] ($10^7 M_\odot$) (2)	r_0[c] (kpc) (3)	ρ_0[d] ($M_\odot$ pc^{-3}) (4)	σ[e] (km s^{-1}) (5)	$\rho_0/\rho_{\rm Gal}$[f] (6)
1.....	1.00E+02	1.84E+00	3.85E−02	4.92E+01	2.49E+01
2.....	4.09E+00	8.51E−01	1.58E−02	1.46E+01	1.15E+01
3.....	1.91E+00	1.11E+00	3.29E−03	8.73E+00	2.76E+00
4.....	6.93E+00	6.31E−01	6.60E−02	2.21E+01	9.53E+00
5.....	3.27E+01	1.70E+00	ρ_2	$2\,\sigma_2$	1.15E+01
6.....	1.16E+01	1.20E+00	ρ_2	$(2)^{1/2}\sigma_2$	1.15E+01
7.....	1.44E+00	6.02E−01	ρ_2	$\sigma_2/(2)^{1/2}$	1.15E+01
8.....	5.11E−01	4.26E−01	ρ_2	$\sigma_2/2$	1.15E+01
9.....	5.78E+00	1.21E+00	$\rho_2/2$	σ_2	5.77E+00
10.....	3.34E+00	6.95E−01	$3\rho_2/2$	σ_2	1.73E+01
11.....	2.89E+00	6.02E−01	$2\rho_2$	σ_2	2.31E+01
12.....	2.36E+00	4.91E−01	$3\rho_2$	σ_2	3.46E+01

[a] Model names.

[b] Mass of Plummer model used for the initial distribution of particles in each satellite.

[c] Scale length of Plummer model used for the initial distribution of particles in each satellite.

[d] Central density of Plummer model used for the initial distribution of particles in each satellite. For models 5–12, ρ_2 and σ_2 are the ρ_0 and σ_c of model 2, respectively.

[e] Characteristic velocity dispersion (σ_c) of the satellite (see text). For models 5–12, ρ_2 and σ_2 are the ρ_0 and σ_c of model 2, respectively.

[f] Ratio of the satellite's initial central density to the mean density of the Galaxy ($\rho_{\rm Gal}$) within the pericenter of its orbit.

ruption of a satellite depends on its density (e.g., King's tidal radius formula [King 1962]) and imply that the larger the value of $\rho_0/\rho_{\rm Gal}$ for a satellite on a given orbit, the longer it is likely to survive (see § 2.2).

The first four models (1–4) have satellite and orbit parameters chosen at random to explore a range of possible outcomes. The orbits for each model are plotted in Figure 1. In each case, the X-Y plane is defined by the satellite's initial radius and velocity vectors, and Z is the position perpendicular to this plane. In no case is the X-Y plane coincident with the Galactic disk since the orbital parameters were chosen at random.

The remaining eight models were chosen to isolate dynamical effects arising from the first four cases, using model 2 for comparisons. These models all employ the same orbit as model 2. In models 5–8, the satellites have the same ρ_0 as model 2 but different σ_c. In models 9–12, the satellites have the same σ_c as model 2 but different ρ_0.

All computations were performed on the T3D at the Pittsburgh Supercomputing Center. The parallel structure of the T3D was used to run several simulations at once, one on each node.

2.2. *Tidal Disruption*

Figure 2 shows the bound mass fraction as a function of time for all 12 models. Comparing the time it takes for each model to disrupt ($T_{\rm dis}$) with the last column ($\rho_0/\rho_{\rm Gal}$) of Table 1, we see that $T_{\rm dis}$ increases monotonically with $\rho_0/\rho_{\rm Gal}$. This confirms the use of the density contrast as a general guide to the fragility of a satellite in a given orbit. Models 2 and 5–8 provide a simple demonstration of this trend. These models all employed the same orbit and ρ_0 (and hence $\rho_0/\rho_{\rm Gal}$) while σ_c was varied. In these models, the satellite's masses span a range of nearly 2 orders of magnitude, yet the mass-loss rates for all five are virtually identical.

2.3. *Moving Groups as a Consequence of Disruption*

To characterize how tidal debris disperses in phase space after it has been stripped from a satellite, we examine the particle distribution of each model after 10 Gyr, from a Galactocentric viewpoint, in the (Ψ, v_r)–plane, where Ψ is an angle measured along the great circle defined by the satellite's initial position and velocity, and v_r is radial velocity. Along an orbit, v_r is an oscillatory function of Ψ, with zeros at pericenter and apocenter, and an amplitude determined by eccentricity. In a general spherical potential, the angular period of this radial oscillation is less than 2π and an orbit followed beyond a single radial oscillation is represented in the (Ψ, v_r)–plane by identical curves offset in phase.

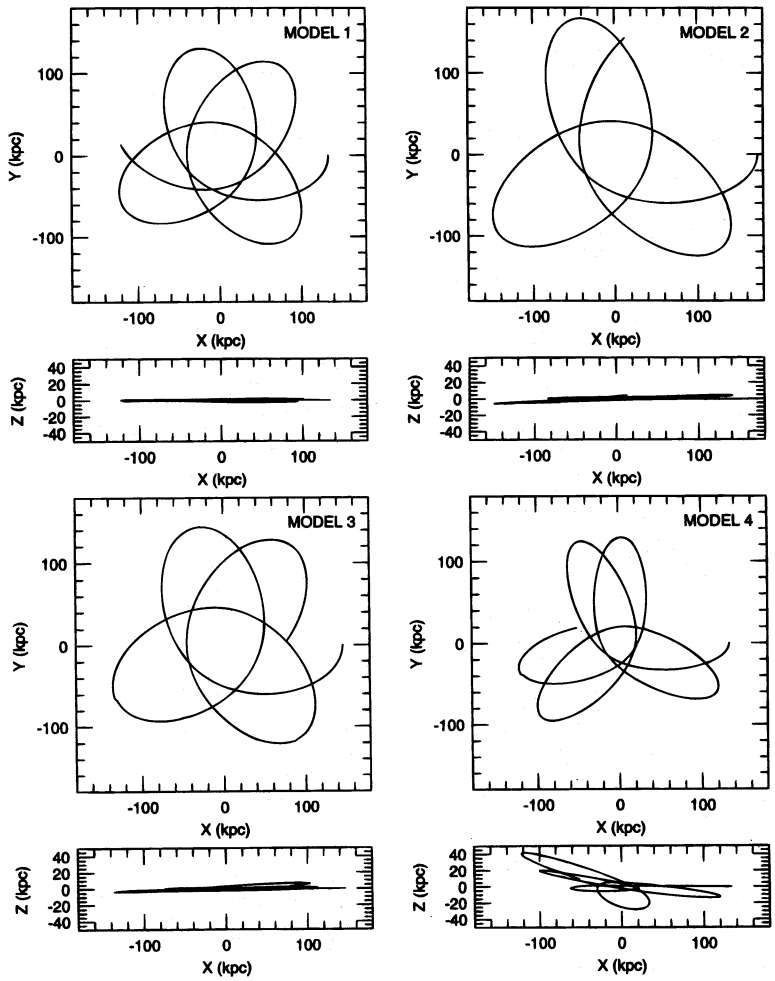

FIG. 1.—Orbits for models 1–4. X and Y are coordinates projected onto the plane defined by the initial position and velocity of the satellite. Z is perpendicular to this plane.

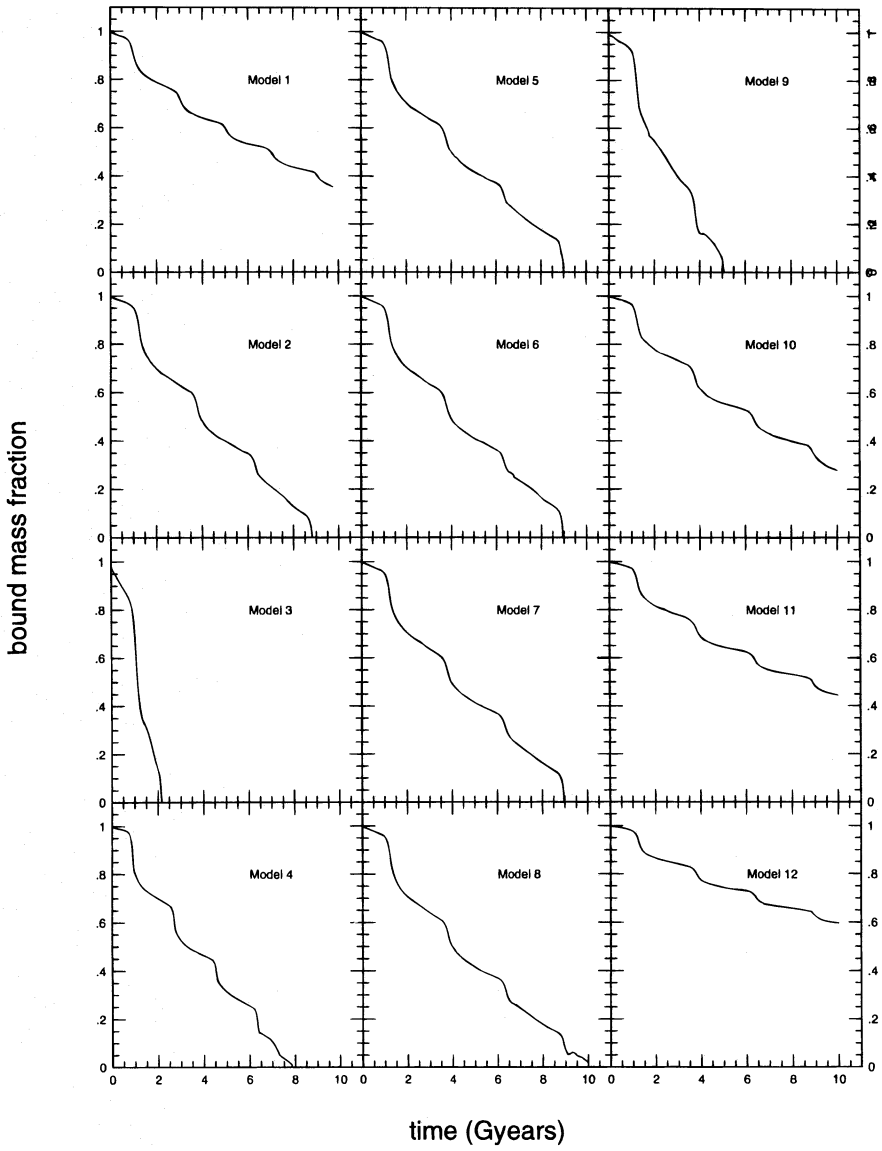

FIG. 2.—Fractional mass bound to each satellite as a function of time for models 1–12

Figure 3 shows contours of the particle density in the (Ψ, v_r)–plane for models 1–12 after 10 Gyr. In all cases, the particles remain in narrow streams over the lifetime of the Galaxy, and the orbits of the satellites can clearly be traced, as described in the previous paragraph. Identical curves offset in phase are seen in models 1 and 5, where the tidal debris has dispersed beyond a single radial oscillation of the orbit.

Figure 3 offers a qualitative assessment of the nature of moving groups associated with each model. Each value of Ψ along a great circle gives the direction of a single line of sight, and the width of the contours in radial velocity Δv_r is a measure of the spread in velocities of the debris along that line of sight. This can vary substantially along a great circle depending on the phase of the orbit sampled by the line of sight, which suggests that moving groups of stars that are related only loosely in distance and radial velocity may still be relics from a single minor accretion event. A systematic trend in velocity with distance should be observed in this case.

2.4. *Debris Dispersal and the Persistence of Alignments*

Figure 4 shows the positions of particles in models 1–4 after 10 Gyr, on a Hammer-Aitoff full-sky projection, where (l, b) are Galactic longitude and latitude from a Galactocentric viewpoint. Note that the debris is aligned along tidal streamers in all cases. In particular, the streamers from model 1, which is nearly on an exactly polar orbit, can be seen to lie along a single great circle outlined by the lines of constant longitude.

Figure 5 shows the fraction of particles at an angular distance δ, perpendicular to each model's great circle, after 10 Gyr. The persistence of alignments of debris along great circles can be assessed by looking at the *width* of this distribution in δ, while the rate of dispersal of debris along the orbit can be seen in the *length* of the tidal streamers in Ψ in Figure 3. Comparing Figures 3 and 5, we find that the extent of the tidal streamers in Ψ is very much greater than in δ, despite the fact that the velocity dispersion in each satellite is isotropic and the debris may (naively) be

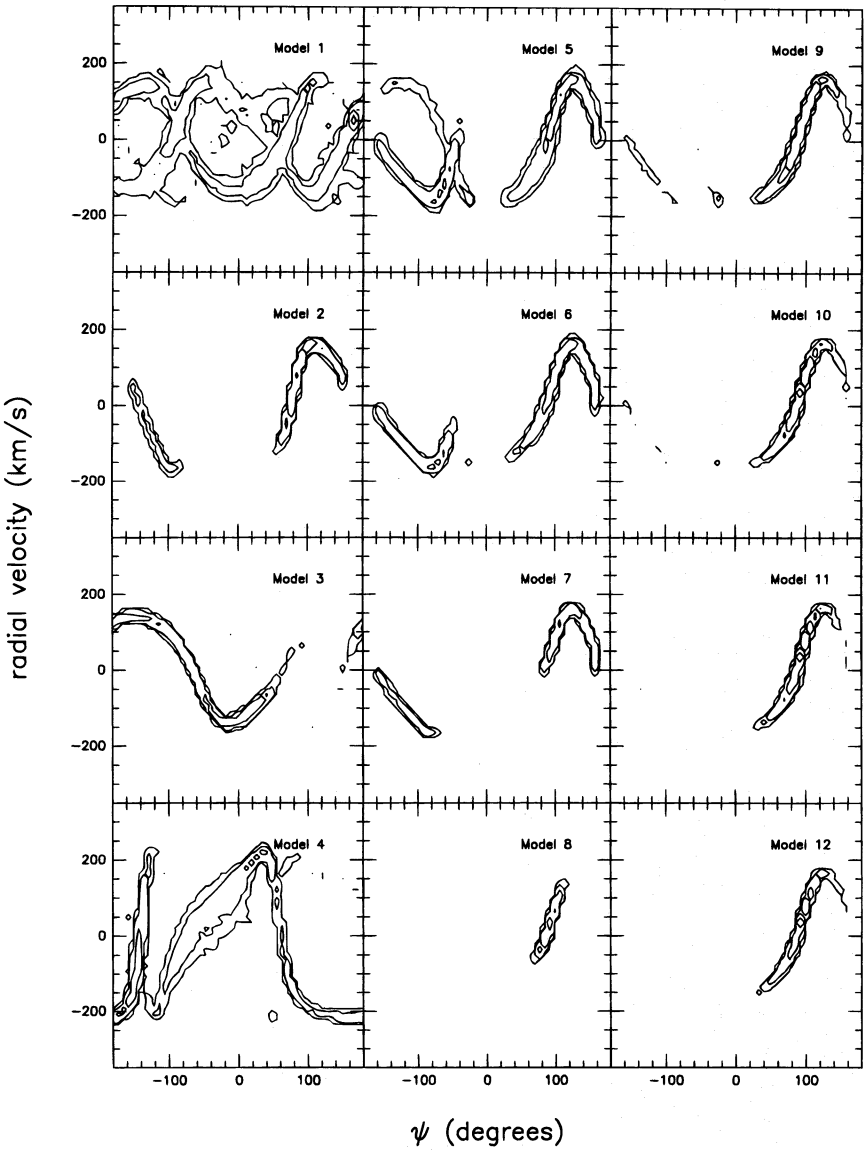

FIG. 3.—Contours of particle density in ψ-v_r space, where v_r is the radial velocity with respect to the center of the Galaxy, and ψ is the angle along the great circle defined by the satellite's initial position and velocity.

expected to disperse over similar distances in any direction. However, the extent of the debris in both δ and Ψ increases with σ_c of the parent satellite: Models 5–8 have identical fractional mass-loss rates and orbits, yet the debris covers a progressively smaller range in δ and Ψ as σ_c decreases; models 9–12 have different fractional mass-loss rates along identical orbits, yet the debris covers a similar range in δ and Ψ since σ_c is constant for these models.

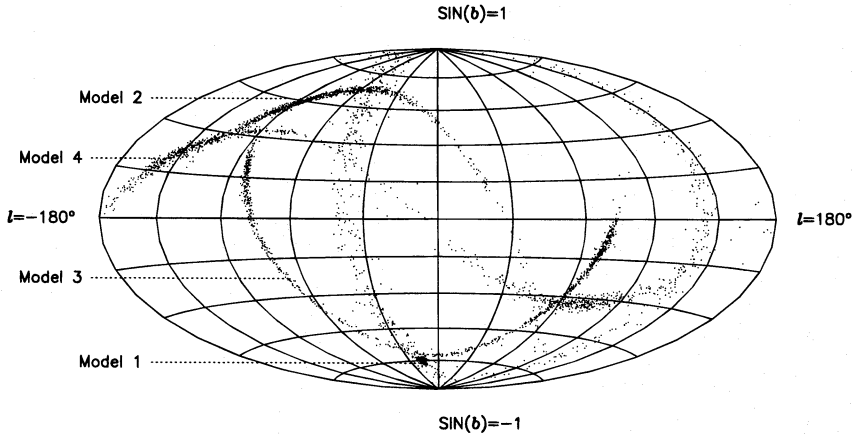

FIG. 4.—Hammer-Aitoff full-sky projection of the positions of particles from models 1–4 after 10 Gyr, in Galactocentric longitude l and latitude b

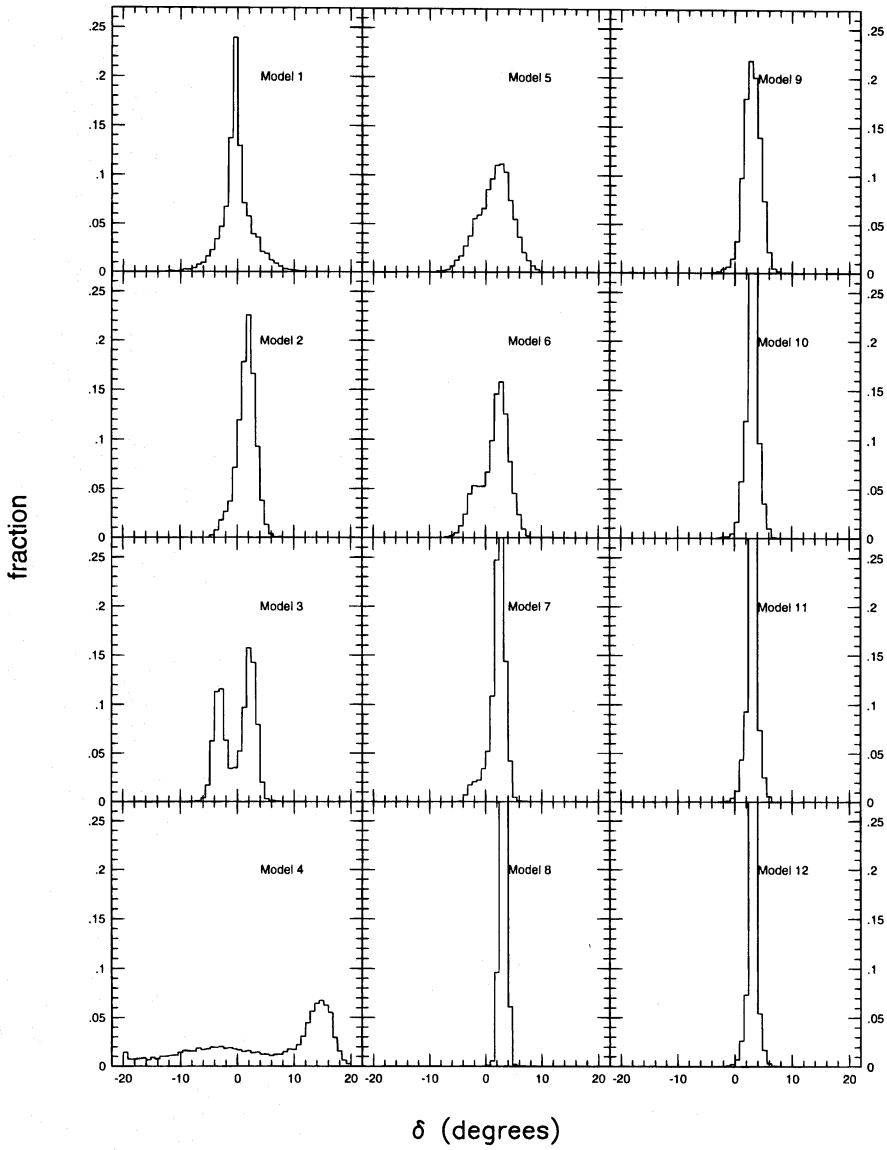

FIG. 5.—Number fraction of particles at an angle δ from the great circle defined by the satellite's initial position and velocity in bins of $\Delta\delta = 1°$

These characteristics of debris dispersal can be explained physically by analogy to the orbits of test particles in a logarithmic potential which has a constant circular velocity, v_c, over all radii. For simplicity, consider a particle initially on a circular orbit at radius R and angular velocity $\Omega = v_c/R$, and define polar coordinates (R, ϕ) to lie in the orbit plane and z perpendicular to it. If the velocity of this particle is perturbed by an amount $\Delta v = \alpha v_c$ (where $|\alpha| \ll 1$), its subsequent motion can be represented using epicycles, with the particle performing independent simple harmonic oscillations in the R, ϕ and z directions about a guiding center on a circular orbit (see, e.g., Binney & Tremaine 1987). The restoring force for these oscillations is provided by the effective potential in this frame, which arises from a combination of the gravitational field and the centrifugal force due to the rotating coordinate system. If the velocity perturbation is only in the z-direction, its new orbit can be described by an oscillation, of z-amplitude αR, about a guiding center following the undisturbed circular orbit. If instead its velocity is perturbed in the ϕ-direction, the new orbit can be described by an oscillation, of radial amplitude $[(\alpha/2)/(1 - \alpha/2)]R$ around a new guiding center on a circular orbit at radius $[1/(1 - \alpha/2)]R$, which moves with angular velocity $(1 - \alpha/2)\Omega$. Hence, if a satellite with characteristic dispersion σ_c were disrupted along the initial circular orbit, after n orbits we may expect the debris to extend over an angular distance $\alpha \propto \sigma_c/v_c$ in δ and $2\pi\alpha n$ in Ψ . A similar argument can explain the radial extent of the debris. Of course, the orbits used in our simulations are far from circular. Figure 6 shows a planar test particle orbit in the potential given by equations (1)–(3) (panels *a–e* [*solid lines*]). The dotted lines show orbits disturbed by $\Delta v = \pm 0.2v$ (where v is the initial velocity of the unperturbed orbit) in the R- (panels *a* and *b*), ϕ- (panels *c* and *d*), and z- (panels *e* and *f*) directions. The qualitative behavior is identical to that expected for perturbations from a circular orbit, with the particle oscillating about a guiding center on the original orbit for R and z perturbations but evolving to a different orbit with a distinct azimuthal period for perturbations in the ϕ-direction.

The one exception to this picture is model 4, the debris from which spreads over a wide range in δ despite its relatively low σ_c. A simple explanation is provided by Figure 1,

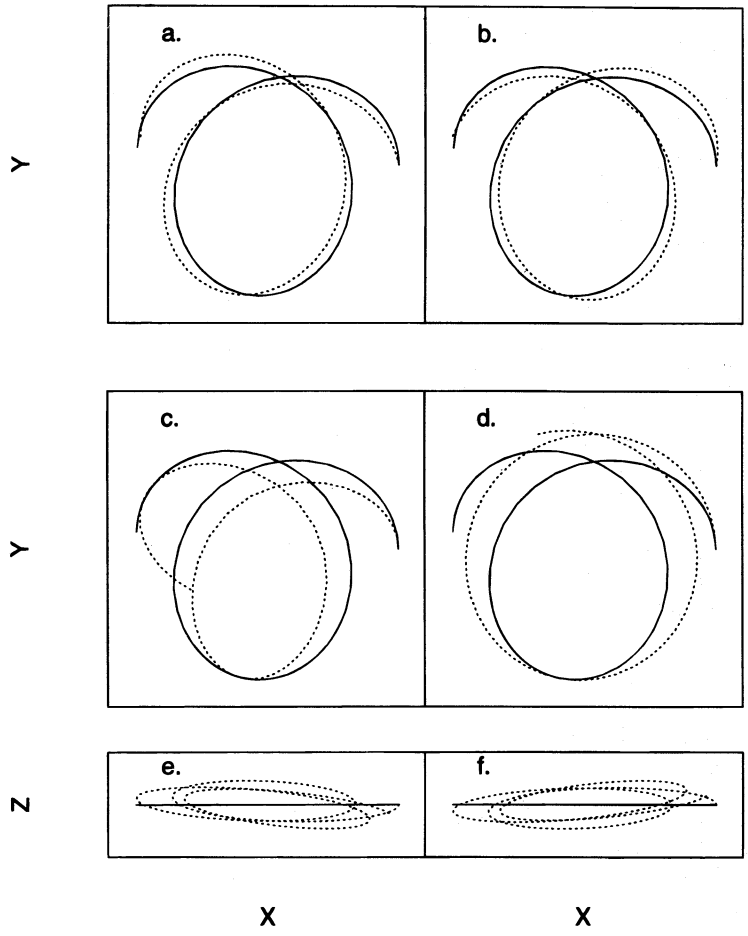

FIG. 6.—Rosette orbit in the potential given by eqs. (1)–(3) (*solid line*) compared to one perturbed by $\Delta v = \pm 0.2v$ (*dotted line*) in (*a* and *b*) the *R*-, (*c* and *d*) ϕ-, and (*e* and *f*) *z*-directions, where v is the initial velocity of the undisturbed orbit.

which shows that the orbit of model 4 orbit is far from planar, since its pericenter is smaller than the other models and its orbit precesses because of the nonspherical potential of the disk. Hence, although Figure 3 suggests that debris from this interaction remains well correlated in streamers, the orbit itself oscillates around the original great circle plane, spreading the debris to large δ, as seen in Figure 5.

We conclude that debris trails can remain aligned in streamers near the parent satellite's original orbit over the lifetime of the Galaxy if σ_c is not comparable to the orbital velocity. If the orbit itself is near planar, the trails may coincide with great circles in the sky.

3. GREAT CIRCLE CELL COUNTS (GC3): A METHOD FOR DETECTING DEBRIS TRAILS

3.1. *Method*

In a spherical halo model, we find that debris trails from the disruption of a satellite can remain aligned along the great circle associated with the satellite's orbit for many Gyr (see § 2). The method of great circle cell counts (hereafter GC3) is designed to search for this distinctive structure in a survey of halo stars, where the stars associated with a debris trail may contribute a negligible fraction of the total surface density.

A great circle cell is defined by the direction of its pole relative to the north Galactic pole, given by the two angles (θ, ϕ), and a width, $2 \times \delta\theta$, as illustrated in Figure 7. A grid of great circle cells is chosen, the poles of which are equally spaced in the intervals $-\pi < \phi < \pi$ and $0 < \cos(\theta) < 1$, to provide a systematic search for debris trails along all possible great circles. The fraction of sky covered by any one cell is $p = \delta\theta$. Hence, if N stars are distributed at random on

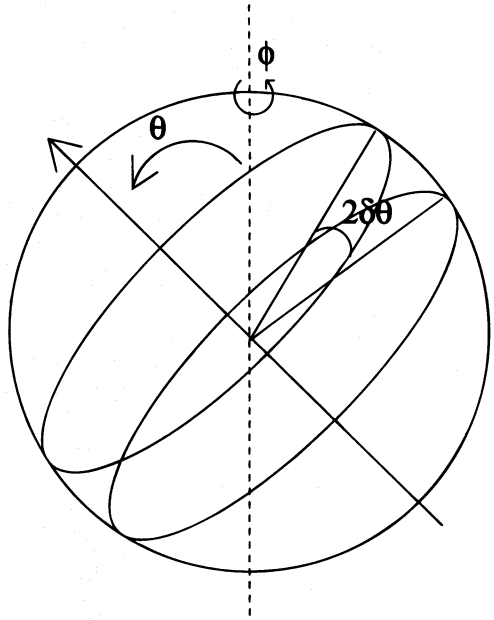

FIG. 7.—Great circle cell, defined by the position of its pole relative to the symmetry axis of the Galaxy.

the sky, the number of stars to fall in a cell follows a binomial distribution (N, p), with a predictable average $\bar{N} = Np$ and dispersion $\sigma_{ran} = [Np(1-p)]^{1/2}$. If some fraction of the N stars are distributed preferentially along a particular great circle, with pole (θ_0, ϕ_0), the counts in the cell whose pole is closest to (θ_0, ϕ_0) will be a local maximum, and the dispersion, σ, of counts will be greater than that predicted for an isotropic distribution, σ_{ran}.

3.2. *Results*

We tested GC3 on artificial halo distributions containing N_{ran} points distributed isotropically on the sky and N_{sat} debris trails. Each trail was based on a set of 200 points taken from the final distribution of particles in the satellite with the shortest disruption time—and hence the longest time for debris to disperse—model 3. To construct N_{sat} different trails, the set of chosen points was rotated N_{sat} times, assuming the influence of the disk on the evolution of model 3 to be negligible. For all our calculations, we used a 51 × 51 grid of great circle cells with width $\delta\theta = 0.02$ and poles equally spaced in [cos (θ), ϕ]–space. The significance of the deviation of the counts N_{count} in any one cell from a random distribution was quantified by defining

$$\mathrm{GC3} = (N_{count} - \bar{N})/\sigma_{ran} . \quad (5)$$

As a simple test of the method, we created an artificial halo containing a single debris trail and $N_{ran} = 19{,}800$ particles from a random distribution and applied GC3 from a Galactocentric viewpoint. Figure 8*a* shows the contours of the cell counts at levels GC3 = 0 (*dotted*), 4, 5, and 6 (*solid*). The cross marks the maximum in GC3. Figure 8*b* demonstrates that positions of particles in model 3 closely follow the great circle associated with this cell.

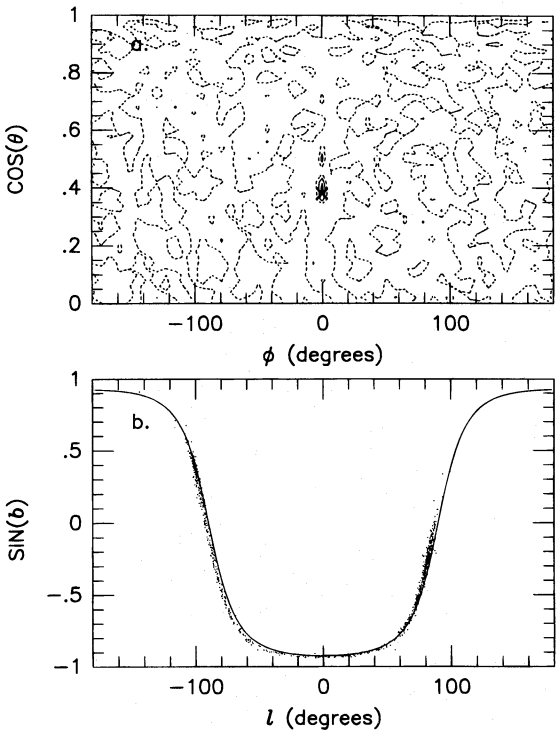

FIG. 8.—(*a*) Contours of GC3 (eq. [5]) on a 51 × 51 grid of poles in [cos (θ), ϕ] (see Fig. 7) at levels 0 (*dotted*), 4, 5, and 6 (*solid*) for the Galactocentric view of an artificial halo distribution containing 1% of its particles in a single debris trail. The cross marks the maximum in the cell counts. (*b*) Positions of particles in the trail in Galactic longitude l and latitude b, compared to the great circle recovered from (*a*).

In Figure 9 we test the ability of GC3 to recover great circles from the Galactocentric view of a halo containing $N_{sat} = 10$ debris trails, with a background of $N_{ran} = 18{,}000$ stars. In Figure 9*a*, the crosses mark all local maxima above GC3 = 3, and the numbers label the maxima in decreasing order of significance. Figure 9*b* shows that each of the N_{sat} debris trails can be associated with great circles recovered from the cell counts.

Unfortunately, we do not have a Galactocentric view of our own halo. Figure 10*a* shows contours of GC3 from the heliocentric view of the distribution used in Figure 9, and Figure 10*b* shows that nine of the 10 debris trails are still successfully recovered. However, the extent of the distortion of a debris trail away from its great circle because of the heliocentric offset will depend on the ratio of the distance of the Sun away from the plane of the great circle to the distance of stars in the trail, and trails at smaller distances (the pericenter of the orbit in our case was >20 kpc) could be more seriously affected.

In Figure 11 we test the sensitivity of GC3 by examining how the dispersion in the counts behaves for the same distribution of accreted material used in Figures 9 and 10 but with an increasing background of randomly placed stars. The error bars for each point represent the standard deviation in the dispersion, calculated from 10 different realizations of an artificial halo, each containing the same number of debris trails and isotropically distributed particles. The points correspond to surveys in which 10%, 5%, 2%, and 1% of the stars are relics from accretion events (or each debris trail contains 1%, 0.5%, 0.2%, and 0.1% of the stars

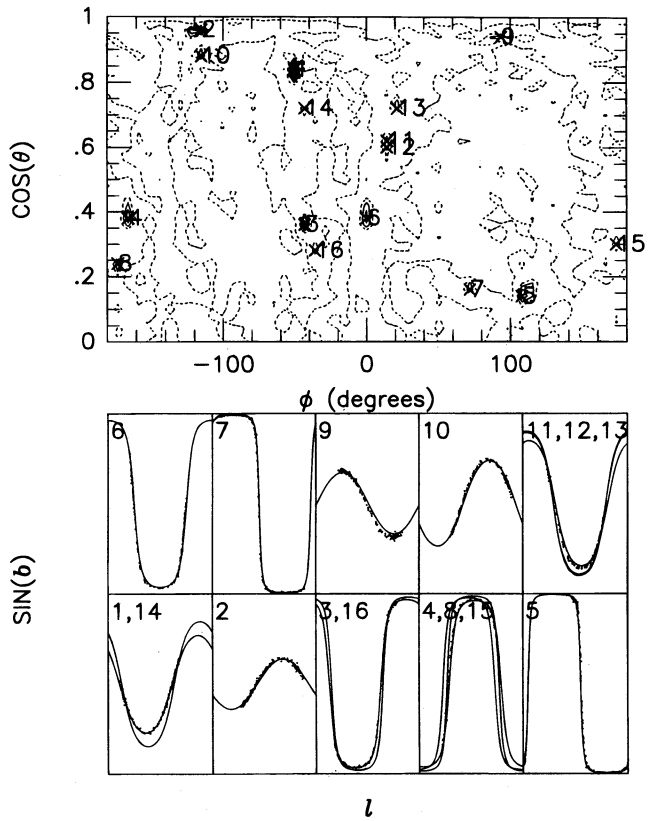

FIG. 9.—(*a*) As Fig. 8*a*, but for an artificial halo containing 10 debris trails, which each contribute 1% of the particles in the distribution. The crosses mark all local maxima above GC3 = 3, and the numbers give the relative importance of each maxima. (*b*) Positions of each debris trail compared to the most closely associated great circles recovered from a.

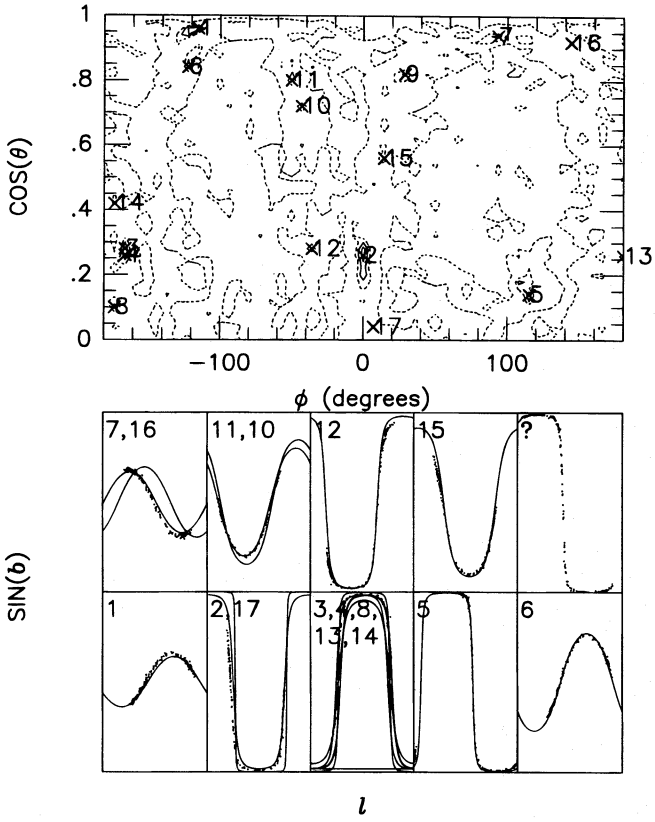

FIG. 10.—As Fig. 9, but for the heliocentric view of the same distribution.

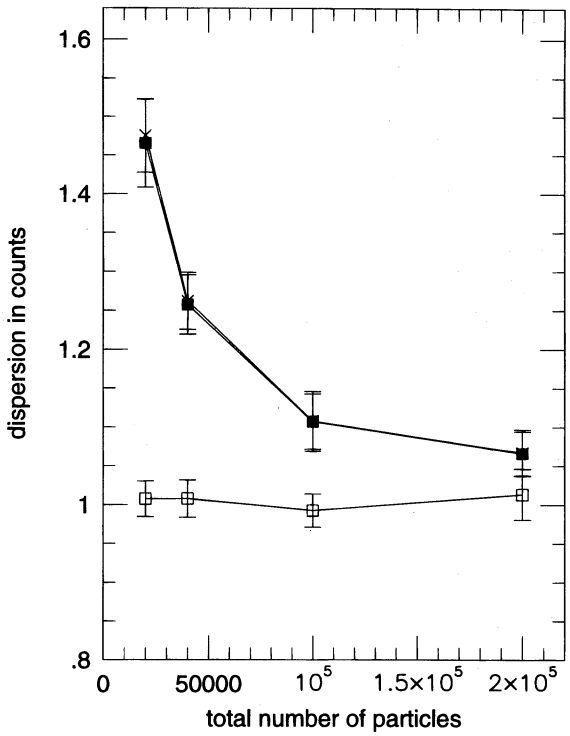

FIG. 11.—Dispersion in the cell counts for the Galactocentric (*crosses*) and heliocentric (*filled squares*) view of artificial halos containing the same debris trails as in Fig. 9, but with an increasing number of background stars ($N_{tot} = N_{ran} + 2000$) or decreasing percentage of accreted material. The open squares give the values for a random distribution of N_{tot} stars. The error bars give the standard deviation calculated from 10 different realizations of artificial halos with the same number of debris trails and background stars.

surveyed). From both Galactocentric (*crosses*) and heliocentric (*filled squares*) viewpoints, the dispersion is significantly different from an isotropic one (*open squares*) in all but the last case.

In summary, the results from this section suggest that GC3 may be used to recover great circles associated with debris trails. The dispersion in GC3 can provide a statistical measure of such structure in a survey of halo stars. In § 5 we discuss the application of this method to a real survey, the effect of an oblate halo on our results, and the possible inclusion of velocity information in the method.

4. OTHER MEASURES OF STRUCTURE

We applied other measures of structure, analogous to tests used in cosmological surveys and for characterizing fluctuations in the cosmic microwave background, to artificial halo distributions with some success.

We mapped the distributions onto a grid of cells equally spaced in [sin (b), l] and found that the dispersion in the counts differed significantly from a random distribution if as few as 1% of the stars were taken from debris trails. This test proved to be as sensitive as GC3 to the presence of substructure but had the disadvantage of not being able to distinguish between general clumpiness and inhomogeneities specifically associated with accretion events.

Following Doinidis & Beers (1989), we calculated the angular correlation function, $C(\beta)$, of the distributions by counting particle pairs separated by an angle β and found an excess of pairs at small angles for halos containing at least 10% debris. This result is interesting in that it suggests that the detection by Doinidis & Beers of power on small scales could result only from a significant deviation from isotropy, but again, the test fails to distinguish between clumpiness and accreted structure.

Last, we calculated the Legendre polynomial (P_l) decomposition of the correlation function

$$C(\beta) = \sum_l \frac{2l+1}{4\pi} A_l^2 P_l[\cos(\beta)] \qquad (6)$$

directly from the angular distribution of the stars (see Peebles 1993). We found that for halos containing a single debris trail, the coefficient of the even terms in the expansion were an order of magnitude larger than the odd terms. Increasing the isotropic background increased the power in only the monopole term. This signature results from the fact that the correlation function is a constant for an isotropic distribution and an even function for a constant density band along a great circle. Unfortunately, the test proved impractical for any realistic situation, since the enhancement of the even coefficients was lost with the introduction of more than one debris trail to the distribution.

5. DISCUSSION

From our simulations of satellite accretion, which were run assuming a Milky Way model having a spherical halo, we find that debris from interactions can remain aligned in tidal streamers, close to the parent satellite's original orbit, for the lifetime of the Galaxy. If the orbit is near planar, the projected path of the streamers may be closely associated with a single great circle. The method of GC3 exploits this characteristic to recover multiple debris trails from artificial halos containing $\geq 1\%$ of material accreted from any single satellite. The dispersion in the counts may be used to quantify the significance of such structure in a distribution con-

taining an even smaller percentage of accreted material and possibly as an indicator for the role that accretion has played in the formation and evolution of the Milky Way.

Some of these conclusions may depend on our assumption of a spherical halo. There is growing evidence for the oblateness of galactic halos in general (see, e.g., Sackett & Sparke 1990; Sackett et al. 1994a, b) and our own in particular (see, e.g., Larson & Humphreys 1994), and nonplanar orbits in such a potential may destroy the alignments with great circles seen in our simulations. However, for orbits in moderately flattened potentials, the total angular momentum is approximately constant, and the z-component of the angular momentum is exactly conserved (see, e.g., Binney & Tremaine 1987). Hence, the orbit lies near a plane the pole of which maintains a constant angle, θ, with the symmetry axis while precessing in ϕ about it (see Fig. 7). This suggests that we may still detect structure characteristic of tidal debris on our grid of poles of great circles in [cos (θ), ϕ], either directly or by summing over cells with constant θ. Debris from satellites on orbits with pericenters somewhat smaller than the ones in our models, which precess because of the axisymmetric potential of the disk, may also be recovered in this manner.

We base our conclusions on "all-sky surveys" of our artificial halos. In practice, it may be difficult to use GC3 at low Galactic latitudes ($|b| < 15°$) because of the predominance of disk stars and inhomogeneity of absorption by the interstellar medium near the Galactic plane. However, GC3 could equally well be applied to a restricted survey, since the area of intersection of any great circle cell with a given region (or regions) of sky can always be calculated. The average and dispersion in the number of stars to fall in that area from a random distribution of stars in the region can be predicted, and the significance of the counts (from eq. [5]) can still be assessed. A survey may have to cover a minimum of a few hundred square degrees to detect local structure since we expect tidal debris to span several degrees, while a survey covering a significant fraction of the sky would be required to look at the global structure of the halo.

Finally, our chances of detecting debris could only be improved with the addition of velocity or distance information. Proper motions could be used to reduce the noise in the cell counts by applying a stricter membership criterion for a cell, defined not only by a star's position but also by the alignment of its velocity vector along the great circle. Alternatively, radial positions and velocities could be used to refine the cell counts, using our knowledge that these quantities should oscillate in Ψ along a great circle, with a period $P < 2\pi$. The signature of a debris trail in a great circle cell could be detected by systematically searching possible periods for excess power in the quantity $A^2 + B^2$, where

$$A = \sum y \cos(\Psi/P), \quad B = \sum y \sin(\Psi/P),$$

the sum is performed over all particles in the cell, and y is either radial position or velocity. In all three cases, once an overdense cell has been identified, the extra coordinate (proper motion, radial position, or velocity) could be used to recover the parent satellite's content and orbit by identifying coherent streams of stars along this great circle.

To summarize: we propose that the method of GC3 might be used to detect signatures of ancient accretion events in either spherical or oblate halos from surveys covering more than a few hundred square degrees. The ultimate test of this assertion is the application of GC3 to a real survey of halo stars, such as the APM survey (see, e.g., Maddox et al. 1990), the APS survey of POSS-I (see, e.g., Pennington et al. 1993), or the digitized survey of the POSS-II catalog (see, e.g., Weir, Fayyad, & Djorgovski 1995).

We would like to thank David Spergel for helpful discussions and John Dubinski for an introduction to the T3D. This work was supported in part by the Pittsburgh Supercomputing Center, the Alfred P. Sloan Foundation, NASA Theory Grant NAGW-2422, NSF grants 90-18526, ASC 93-18185, and AST 91-17388, and the Presidential Faculty Fellows program.

REFERENCES

Arnold, R., & Gilmore, G. 1992, MNRAS, 257, 225
Barnes, J. E. 1988, ApJ, 331, 699
———. 1992, ApJ, 393, 484
Binney, J., & Tremaine, S. 1987, Galactic Dynamics (Princeton: Princeton Univ. Press)
Croswell, K., Latham, D. W., Carney, B. W., Schuster, W., & Aguilar, L. 1991 AJ, 101, 2078
Doinidis, S. P., & Beers, T. C. 1989, ApJ, 340, L57
Eggen, O. J., Lynden-Bell, D., & Sandage, A. R. 1962, ApJ, 136, 748 (ELS)
Fusi Pecci, F., Bellazzini, M., Cacciari, C., & Ferraro, F. R. 1995, AJ, 110, 1664
Grillmair, C. J., Freeman, K. C., Irwin, M., & Quinn, P. J. 1995, AJ, 109, 2553
Hernquist, L. 1990, ApJ, 356, 359
———. 1992, ApJ, 400, 460
———. 1993, ApJ, 409, 548
Hernquist, L., & Ostriker, J. P. 1992, ApJ, 386, 375
Hibbard, J. E., & Mihos, J. C. 1995, AJ, 110, 140
Ibata, R. A., Gilmore, G., & Irwin, M. J. 1994, Nature, 370, 194
Johnston, K. V., Spergel, D. N., & Hernquist, L. 1995, ApJ, 451, 598
King, I. R. 1962, AJ, 67, 471
Larson, J. A., & Humphreys, R. M. 1994, ApJ, 436, L149
Larson, R. B. 1990, PASP, 102, 709
Lin, D. N. C., & Richer, H. B. 1992, ApJ, 388, L57
Lynden-Bell, D. 1976, MNRAS, 174, 695
———. 1982, Observatory, 102, 202
Lynden-Bell, D., & Lynden-Bell, R. M. 1995, MNRAS, 275, 429
Maddox, S. J., Sutherland, W. J., Efstathiou, G., & Loveday, J. 1990, MNRAS, 243, 692
Majewski, S. R. 1993, ARA&A, 31, 575
———. 1994, ApJ, 431, L17
Majewski, S. R., Munn, J. A., & Hawley, S. L. 1994, ApJ, 427, L37
McGlynn, T. A. 1990, ApJ, 348, 515
Miyamoto, M., & Nagai, R. 1975, PASJ, 27, 533
Peebles, P. J. P. 1993, Principles of Physical Cosmology (Princeton: Princeton Univ. Press)
Pennington, R. C., Humphreys, R. M., Odewahn, S. C., Zumach, W., & Thurmes, P. M. 1993, PASP, 105, 521
Piatek, S., & Pryor, C. 1995, AJ, 109, 1071
Plummer, H. C. 1911, MNRAS, 71, 460
Sackett, P. D., Morrison, H. C., Harding, P., & Boroson, T. A. 1994a, Nature, 370, 441
Sackett, P. D., Rix, H. W., Jarvis, B. J., & Freeman, K. C. 1994b, ApJ, 436, 629
Sackett, P. D., & Sparke, L. S. 1990, ApJ, 361, 408
Searle, L., & Zinn, R. 1978, ApJ, 225, 357 (SZ)
Sommer-Larsen, J., & Christiansen, P. R. 1987, MNRAS, 225, 499
Spergel, D. N. 1996, in preparation
Toomre, A., & Toomre, J. 1972, ApJ, 178, 623
Tóth, G., & Ostriker, J. P. 1992, ApJ, 389, 5
Vandenberg, D. A., Bolte, M., & Stetson, P. B. 1990, AJ, 100, 445
Weir, N., Fayyad, U. M., & Djorgovski, S. G. 1995, AJ, 109, 2401